Intra-seasonal variability of extreme boreal stratospheric polar vortex events and their precursors

Adelaida Díaz-Durán[1], Encarna Serrano[1], Blanca Ayarzagüena[2], Marta Abalos[3] and Alvaro de la Cámara[3]

Affiliation:

[1] Universidad Complutense de Madrid, Madrid, Spain

[2] College of Engineering, Mathematics and Physical Sciences, University of Exeter, Exeter, United Kingdom

[3] National Center for Atmospheric Research, Boulder, Colorado, United States

Corresponding author:

Adelaida Díaz-Durán, Dpto. Geofísica y Meteorología, Facultad de CC. Físicas, Universidad Complutense de Madrid, Madrid, Spain.

e-mail: adelaidadiazduran@ucm.es

Abstract

The dynamical variability of the boreal stratospheric polar vortex has been usually analysed considering the extended winter as a whole or only focusing on December, January and February. Yet recent studies have found intra-seasonal differences in the boreal stratospheric dynamics. In this study, the intra-seasonal variability of anomalous wave activity preceding polar vortex extremes in the Northern Hemisphere is examined using ERA-Interim reanalysis data. Weak (WPV) and strong (SPV) polar vortex events are grouped into early, mid- or late winter sub-periods depending on the onset date. Overall, the strongest (weakest) wave-activity anomalies preceding polar vortex extremes are found in mid- (early) winter. Most of WPV (SPV) events in early winter occur under the influence of east (west) phase of the Quasi-Biennial Oscillation (QBO) and an enhancement (inhibition) of wavenumber-1 wave activity (WN1). Mid- and late winter WPV events are preceded by a strong vortex and an enhancement of WN1 and WN2, but the spatial structure of the anomalous wave activity and the phase of the QBO are different. Prior to mid-winter WPVs the enhancement of WN2 is related to the predominance of La Niña and linked to blockings over Siberia. Mid-winter SPV events show a negative phase of the Pacific-North America pattern that inhibits WN1 injected into the stratosphere. This study suggests that dynamical features preceding extreme polar vortex events in mid-winter

should not be generalized to other winter sub-periods.

Keywords

Intra-seasonal variability; wave activity; stratospheric polar vortex extremes; tropospheric precursors; tropospheric forcing; stratospheric dynamics.

1 Introduction

The boreal stratospheric polar vortex is perturbed by a variety of forcings, such as the Quasi-Biennial Oscillation (QBO) (Holton and Tan 1980), El Niño-Southern Oscillation (ENSO) (Manzini et al. 2006; Taguchi and Hartmann 2006; Butler and Polvani 2011), tropospheric blockings (Martius et al. 2009; Woollings et al. 2010; Barriopedro and Calvo 2014; Ayarzagüena et al. 2015) or the Arctic sea ice content (García-Serrano et al. 2015; Kolstad et al. 2015). All these studies are based on observations apart from Taguchi and Hartmann (2006) and Ayarzagüena et al. (2015), which are modelling works and Manzini et al. (2006), Wollings et al. (2010) and Kolstad et al. (2015) that combine both. The previously cited forcings modulate the upward wave activity entering the stratosphere that leads to stratospheric polar vortex anomalies (Palmer 1981; Li et al. 2007; Solomon 2014). In particular, an anomalously weak polar vortex (WPV, hereafter) is preceded by a strong upward wave activity from the troposphere causing warming over the stratospheric polar region and weakening of the polar cyclonic circulation (Limpasuvan et al. 2004; Polvani and Waugh 2004). The opposite is true for strong polar vortex events (SPV hereafter, Christiansen 2001). The most dramatic weak vortex regime in the Northern Hemisphere (NH) winter is called major stratospheric warming (MSW), during which polar temperature increases dramatically in a few days, the equator-pole temperature gradient reverses and the zonal-mean flow becomes easterly (Andrews et al. 1987).

The importance of the occurrence of these stratospheric extreme events for the tropospheric climate variability has been long documented (Baldwin and Dunkerton 1999, 2001), and several studies have shown an improvement of seasonal forecasts based on stratospheric information using different models or statistical methods (Christiansen 2005, Scaife et al. 2014).

Typically, changes in the boreal polar vortex and its dynamics have been analysed by considering the whole extended winter (from November to March) or only focusing on the most dynamically active months (December, January and February) as representative of the winter season (Kodera et al. 2003). Recent studies have consistently shown intra-seasonal differences in the dynamics of the extended boreal winter. Using a chemistry-climate model (CCM), Ayarzagüena et al. (2013) identified a different polar stratospheric response to future changes in early winter and mid-to-late winter under projected climate change scenarios. This work showed that, even though there are no statistically significant future changes in the mean frequency of MSWs, there is a shift in the occurrence of this phenomenon with more events registered in mid- and late winter in a

future climate. Solomon (2014) classified the episodes of enhanced wave activity (WAEs) into four categories in a decreasing sequence according to its magnitude (major, minor, final and other WAEs) and identified their most common timing. Major WAEs are more likely to occur during mid-winter, minor WAEs are recorded throughout the extended winter, final WAEs occur most likely in late winter, and the other WAEs predominate in early winter. Nevertheless, Solomon (2014) did not explore the reasons for the variability in wave activity among winter sub-periods and the potential precursors in each type of episodes. The goal of the present paper is to analyse the intra-seasonal variability of stratospheric anomalous circulation in the NH, and to gain insight into the dynamical mechanisms driving the extreme polar vortex events in different periods throughout the extended NH winter.

The structure of this paper is as follows. Section 2 describes the data and methodology used in this work to identify extreme polar vortex events and to study the corresponding anomalous tropospheric wave-activity propagation. In section 3 we show and discuss intra-seasonal differences in the wave-activity climatology, as well as differences in the anomalous wave activity and anomalous circulation structures prior to WPV and SPV events in three winter sub-periods (early, mid- and late winter). Finally, in section 4, we include a summary with the main conclusions derived from our work.

2 Data and methodology

We use daily-mean data of the three wind components, temperature and geopotential height from ERA-Interim reanalysis (Dee et al. 2011), calculated by averaging the 6-hourly data, for the period 1979-2011. The data extends from 1000 to 1 hPa (37 levels) and the spatial domain is the Northern Hemisphere (NH) and the subtropical region of Southern Hemisphere (20ºS-90ºN, 180ºW-180ºE) on a 1.5º×1.5º grid.

The analysis has been restricted to post-satellite era in order not to combine post and pre-satellite data that might lead to misleading results. For instance, Gomez-Escolar et al. (2012) found differences in the polar stratospheric temperature climatology in mid-winter between pre-satellite and post-satellite eras, which might be related to satellite data assimilation. Consequently, ERA-Interim has been used despite covering a shorter period than other currently reanalysis datasets (e.g.: JRA-55 or NCEP-NCAR).

2.1 Extreme polar vortex events

In this work, the strength of the stratospheric polar vortex is quantified by using daily values of zonal mean

zonal wind at 60ºN (denoted as $\overline{u_{60}}$) and 10 hPa. The central date (day 0) of a WPV is defined as the first day that $\overline{u_{60}}$ at 10 hPa falls below its daily 15th percentile according to the corresponding daily climatology over 1979-2011. In the case of SPV events, its central day is identified as the first day that $\overline{u_{60}}$ at 10 hPa reaches out its daily 85th percentile (Fig.1a). Note that percentiles 15th and 85th are a proxy of the mean value of minus and plus one standard deviation, respectively, in a Gaussian distribution (although we note this might not be the case for this data). These events should persist at least 10 days to be considered as extreme events. In addition, two consecutive extreme events are taken as independent events if there are at least 10 days between the disappearance of the former and the onset of the latter. The 10-day interval corresponds approximately to the wintertime radiative relaxation time scale at 10 hPa and 60ºN (Newman and Rosenfield 1997).

We distinguish WPV and SPV events occurred in October-November-December (OND, early winter), in January-February (JF, mid-winter) and in March-April (MA, late winter). The reason of including October in early winter, unlike other studies, is because the polar vortex has already formed according to the geopotential height at 50 hPa. In addition, October has the same number of hours of sunshine as April, which is usually considered part of the extended winter (Limpasuvan et al. 2004; Kolstad et al. 2015). With these criteria, we have registered 33 WPV (15 in OND, 9 in JF and 9 in MA) and 32 SPV events (17 in OND, 11 in JF and 4 in MA) (Table 1). Note that 8 out of the 9 WPV events which occurred in mid-winter (JF) satisfy the MSW conditions, i.e., the meridional temperature gradient at 10 hPa between 60ºN and the North Pole reverses and $\overline{u_{60}}$ at 10 hPa becomes easterly (Quiroz 1979; Labitzke 1981). The distribution of WPV and SPV events under the different ENSO and QBO phase is shown in Fig.1b and Fig.1c, respectively. ENSO and QBO information has been taken from NOAA webpages, namely http://www.cpc.ncep.noaa.gov/products/analysis_monitoring/ensostuff/ensoyears_ERSSTv3b.shtml and http://www.cpc.noaa.gov/data/indices/, respectively.

2.2 Wave activity propagation

We investigate the anomalous wave activity propagation and its effect on the mean stratospheric flow in NH winter the week (average of the 7 days) prior to the occurrence of SPVs and WPVs in each winter sub-period, by computing composites of the corresponding anomalies of Eliassen-Palm flux and its divergence (Eliassen-Palm 1961).

The analysis of the anomalous upward wave propagation is completed by means of the anomalous meridional eddy heat flux $(v'T')_a$ at 100 hPa (proportional to the vertical component F_z of E-P flux) the week prior to the occurrence of SPV and WPV. Hu and Tung (2003) demonstrated that $(v'T')$ averaged over the extratropics at 100 hPa gives a good measure of the tropospheric wave injection into the stratosphere. We calculate the $(v'T')_a$ at 100 hPa averaged over 45ºN-75ºN for all zonal wavenumbers and the first two zonal wavenumbers (k=1, 2) using Fast Fourier Transform filters.

Since we search for the main regions responsible for the change in the tropospheric wave injection into the stratosphere, we also plot not spatially averaged $(v'T')$, which corresponds to a rough approximation of the vertical component of the 3D Plumb Flux (Plumb 1985). As we are interested in dynamical effects of persistent tropospheric circulation structures, daily meridional wind and temperature values have been smoothed out with 5-day running mean in order to identify quasi-stationary waves (Nishii et al. 2009).

The anomalous eddy heat flux has been decomposed into two different components (Nishii et al. 2009; Smith and Kushner 2012):

$$(v'T')_a = (v'_a T'_a)_a + (v'_c T'_a) + (v'_a T'_c) \qquad (1)$$

The subscripts *a* and *c* indicate anomalies and climatological values, respectively. The first right-hand term of Eq.1 corresponds to the nonlinear contribution of anomalous waves, and the sum of the second and the third term indicates the modulation of climatological waves by wave anomalies.

2.3 Statistical significance of results

The statistical significance of the composites is assessed with a Monte Carlo-like test of 5000 samples. Because the composites for each winter sub-period are computed by considering the central date of the extreme events and their respective previous 7 days, each sample is defined as k (number of events) blocks of 8 consecutive days. Central dates of the k events in each sample are selected randomly choosing days and years within each winter sub-period with the condition that the blocks are separated at least 10 days from each other (consistently with our definition of observed strong and weak events).

As an example, to establish the statistical significance of the composite for WPVs in OND (k=15 events), we randomly select 15 non-overlapping blocks from this winter sub-period, that is, among 92 days (from October 1st to 31st December) of 32 years (from 1979 to 2011). The average of the data of these random fifteen 8-days blocks provides one value of the probability distribution function (PDF), and this procedure is repeated 5000

times to construct the full PDF used to establish the statistical significance of the "observed" composite. A two-tailed test is applied with 95% confidence interval based on the obtained PDF.

3 Results and discussion

3.1 Climatological wave activity

We first examine the intra-seasonal variability in the wave activity by analysing the differences between the three winter sub-periods and the extended winter climatological wave activity. Fig.2 displays the cross sections of the climatological E-P flux, its divergence and the zonal wind in a *(ϕ, log (p))* plane for the extended winter, early winter, mid-winter and late winter (i.e. OND, JF and MA).

The climatological E-P flux in the three winter sub-periods is overall similar to the extended winter, but there are relevant differences among them. The wave activity in the subpolar mid-stratosphere is more intense in mid-winter (JF), and the convergence is stronger in the stratosphere (Fig.2c). Consequently, the E-P flux climatology in the extended winter season (Fig.2a) is mainly dominated by the mid-winter months (Fig.2c). In early (Fig.2b) and late winter (Fig.2d), the region of maximum convergence is restricted to the subpolar mid-stratosphere (~10 hPa, 50ºN-60ºN).

The intraseasonal variability in the climatology of the meridional eddy heat flux *(v'T')* at 100 hPa is shown in Fig.3. The largest climatological *(v'T')* at 100 hPa values for the extended winter in the lower stratosphere are found between 50ºN and 70ºN (Fig.3a), in agreement with the cross-section results of vertical component of the E-P flux shown in Fig.2a. There are two regions with large positive meridional eddy heat fluxes, the Eastern Siberia and the Central Siberia, and only one with large negative fluxes in Northwest Canada. Some differences appear among winter sub-periods. The strongest positive *(v'T')* at 100 hPa values located in the easternmost part of Siberia are observed during mid-winter (Fig.3c) and the positive centres over the Scandinavian and Central Siberia present the highest values in late winter (Fig.3d).

3.2 Anomalous wave activity prior to extreme events

3.2.a Zonal mean wave activity propagation

We next study the intra-seasonal differences of anomalous wave activity prior to the identified extreme events among winter sub-periods. Fig.4 (left column) displays the latitude-height composites of the anomalous E-P flux and zonal wind over the week before WPV events. In general for the three winter sub-periods, the wave

activity is stronger than the climatology, with anomalous upward E-P flux and enhanced eddy-induced deceleration of the mean flow in the stratosphere, which highlights the role of planetary waves in forcing WPV events. This interaction between the anomalous wave activity and the winter stratospheric mean flow leads to a weakening of the zonal wind in the extratropical stratosphere before the onset of WPV events. Some differences among winter sub-periods can be observed, with the strongest anomalies of E-P flux, E-P flux divergence, and zonal wind for WPVs occurring in mid-winter (Fig.4c) in agreement with Solomon (2014). In addition, only prior to mid-winter WPVs the statistically significant anomalous wave propagation above 10 hPa extends into the subtropics. In the equatorial stratosphere there is an EQBO-like structure (anomalous easterly winds in the lower stratosphere and westerly winds above them) prior to the occurrence of WPV events in early winter (Fig.4a). To a lesser extent, we can also see an EQBO-like structure for events in mid-winter, and WQBO-like winds for the WPVs in late winter. Although the anomalous equatorial zonal winds are not statistically significant at a 95% confidence level, these vertical structures are in agreement with the statistics on QBO phase and weak vortex events presented in (Fig.1b). The predominance of EQBO for WPVs in early winter (11 out of 15 events) and mid-winter (6 in 9 events) is in agreement with the Holton and Tan (1980) relationship between the QBO and the stratospheric polar vortex state. However, the dominance of WQBO in late winter (6 out of 9 events) eludes this explanation, probably because the transition from WQBO to EQBO occurs primarily in spring/summer season (April-August) (Dunkerton 1990). In this regard, Gray (2003) and Gray et al. (2004) showed in several model experiments that in early winter the polar stratosphere might be more sensitive to the QBO phase. In the later stages of winter, the flow becomes more nonlinear and the influence of subtropical and equatorial upper stratosphere might be more important (Gray et al. 2004). More recently, White et al. (2016) studied the seasonal evolution of the Holton-Tan effect during the extended Northern Hemisphere winter and their results agree well with those of the present study. They showed that under EQBO in early winter there is a stronger meridional circulation in the lower stratosphere and a wave convergence at high latitudes in the middle stratosphere that leads to a weak polar vortex. In mid-February the polar vortex starts to recover from the previous weakening and becomes anomalously strong for that time of the year (White et al. 2016).

The wave activity in the week prior to the SPV onset (Fig.4, right column) is weaker than the climatology, with anomalous downward E-P flux and positive anomalous divergence (i.e. reduced convergence) at mid-

and high latitudes in the three winter sub-periods. As observed for the WPVs, the strongest anomalies of wave activity prior to the SPV events are found in mid-winter (Fig.4d) but the strongest positive anomalies of zonal wind are observed for late winter SPVs in the extratropical stratosphere (Fig.4f). However, this last result must be taken with caution due to the low number of SPV events (only 4) in late winter. Conversely to WPVs, Fig.4b shows the presence of a WQBO structure linked to SPVs in early winter; Fig. 1c already showed that WQBO is present during SPV events in early winter (12 out of 17 cases). Although a WQBO structure is not very evident in mid-winter (Fig. 4d) and late winter (Fig. 4f), 8 in 11 cases in mid-winter and 3 out of 4 cases in late winter occur during WQBO phase. We recognize the limitations of trying to draw conclusions on the potential relation between QBO and extreme vortex events with a small number of cases, but we do report some tendency in the reanalysis data for a particular QBO phase during extreme events identified in early and mid-winter.

3.2.b Vertical wave activity propagation

In order to identify the geographical regions where the anomalous wave activity originates during the week prior to the onset of stratospheric polar vortex extremes, composites of the anomalous meridional eddy heat flux, $(v'T')_a$, at 100 hPa are represented in Fig.5 (WPVs) and Fig.6 (SPVs). Overall, before the onset of WPV events (Fig.5, left column) the climatological behaviour of the wave activity appears reinforced (compare to Fig.3b, Fig.3c, Fig.3d), but with different magnitude on the main regions of wave propagation depending on the winter sub-periods. The smallest anomalies are observed prior to early winter WPVs (Fig.5a), although statistically significant changes are identified over Central Siberia, Bering Sea and Greenland/Northeast Canada regions. In mid-winter, the wave activity over Central Siberia is enhanced before the onset of WPVs (Fig.5d). Additionally, there is a strong injection of wave activity into the stratosphere over the Bering Strait which in mid-winter extends further towards the east over Canada with respect to the climatology (Fig.3c). The climatological negative centre over Northern Canada is intensified (Fig.5g) prior to late winter WPV events. Similarly, the climatological positive ($v'T'$) at 100 hPa (Fig.3d) over Bering Strait and Scandinavian regions significantly increases.

The $v'T'$ at 100 hPa pattern in Fig. 5a is similar to that found by Garcia-Serrano et al (2015) in a study of the influence of Arctic sea ice interannual variability in autumn on the winter (DJF) Euro-Atlantic sea level pressure. In their study, Garcia-Serrano et al. showed that the heat flux pattern appeared as a dynamical

response to Arctic sea ice forcing, and invoked a stratospheric pathway linking sea ice forcing in November and sea level pressure anomalies in DJF. We have plotted a composite map of Arctic sea ice concentration anomalies for our OND weak vortex events, and even though there is a decrease of the Artic sea ice in agreement with García-Serrano et al., the statistical significance is very low (not shown). Therefore, our results are inconclusive about the role of Arctic sea ice forcing the stratospheric variability in early winter.

The central and right-hand columns of Fig.5 show the terms of $(v'T')_a$ at 100 hPa associated with the nonlinear contribution of anomalous Rossby waves and the modulation of climatological waves by wave anomalies, respectively. Overall, the main contribution to the strengthening of the wave activity prior to the WPVs comes from the interaction between climatological and anomalous wave for the three winter sub-periods (Fig.5, right column). This term, $(v'_c T'_a)+(v'_a T'_c)$, also plays an important role over those regions where the wave-activity injection into the stratosphere is weakened prior to mid- and late winter WPVs (Fig.5f, Fig.5i, respectively). Additionally, $(v'_a T'_a)_a$ prior to mid-winter WPVs has a non-negligible contribution to the total $(v'T')_a$; it makes the enhanced wave activity over Bering Strait region extend further eastward (Fig.5e).

The same analysis of the $(v'T')_a$ at 100 hPa preceding the onset of SPVs is shown in Fig.6. As expected, an overall reduction of the climatological wave activity injection into the stratosphere over the main regions of wave propagation is observed for all SPVs occurring in winter (Fig.6, left column). However, intra-seasonal differences in these anomalies are evident, both in magnitude and/or location. For instance, for mid-winter SPV events, the strongest reduction of the wave activity is observed over Alaska and northern Europe (Fig.6d). Interestingly, in mid-winter the spatial structure for SPV events does not match exactly the location of the climatological centres (compare Fig.6d and Fig.3c), while in late winter the spatial pattern weakens the climatological structure (compare Fig.6g and Fig.3d).

Similarly to the WPV events, the term that contributes the most to the $(v'T')_a$ at 100 hPa is associated with the modulation of climatological waves by wave anomalies preceding SPV events (Fig.6, right column). Again there are some differences among winter sub-periods; this term is more intense in mid (Fig.6f) and late winter (Fig.6i).

In order to further explore the intra-seasonal differences in the anomalous wave activity associated with the occurrence of polar vortex extremes, Fig.7 presents the temporal evolution around the onset of these events of

the $(v'T')_a$ at 100 hPa averaged over 45ºN-75ºN considering the separate zonal wavenumber components (wavenumber 1 and 2 (WN1 and WN2, respectively)). In the case of WPVs (Fig.7, left), WN1 component (red line) contributes the most to the preceding enhancement of the extratropical-averaged $(v'T')_a$ at 100 hPa for the three winter sub-periods. However in mid- and late winter, the WN2 component of $(v'T')_a$ at 100 hPa also increases in the week prior to the events (Fig.7c, Fig.7e, green line). Consistently, the pattern of $(v'T')_a$ at 100 hPa displayed in Fig.5d and Fig.5g is a mix of WN1 and WN2 wave patterns; and the pattern of $(v'_cT'_a)$+ $(v'_aT'_c)$ resembles a WN2 pattern (Fig.5f and Fig.5i). One of the possible modulators of WN2 wave activity prior WPVs in mid-winter might be the phenomenon of La Niña. Indeed, 6 out 9 WPV events during mid-winter were preceded by La Niña (Fig.1b). This is consistent with the results of Barriopedro and Calvo (2014) and Li and Lau (2013) regarding the link between ENSO and the zonal wavenumber components prior to weak polar vortex events. In particular, while WPVs that develop during El Niño events tend to be preceded by WN1 wave activity, WPVs that take place during La Niña events tend to be preceded by enhanced WN2 wave activity.

Concerning the wave forcing of SPVs (Fig.7, right column), there is a reduction of the $(v'T')_a$ at 100 hPa averaged over 45ºN-75ºN around the central date of the events mainly due to the WN1 wave component. For both early (Fig.7b) and mid-winter (Fig.7d) events, the negative anomalies grow over time before the SPV onset, but the highest anomalies are observed prior to mid-winter events. Results for late winter SPVs (Fig.7f) showed that the anomalous values always remain negative although they are not statistically significant (only 4 events). This prolonged reduction of wave activity may be because 2 out of 4 late winter SPVs were preceded by WPVs in mid-winter, and the propagation of tropospheric planetary waves is weakened after WPV events during the so-called "late winter cooling period" (Labitzke 1981).

3.3 Anomalous tropospheric circulation structures prior to polar vortex extremes

In this section, we search for a possible link between anomalous middle tropospheric circulation structures and the anomalous wave activity preceding the extreme events of the stratospheric polar vortex already shown. Fig.8 shows composites of the anomalous geopotential height at 500 hPa (Z_{500}) the week before the onset of WPVs and SPVs in the different winter sub-periods. Also, the climatological eddy geopotential height at the same level is included to identify possible constructive or destructive interferences between climatological and anomalous waves associated with the tropospheric circulation anomalies.

a) WPV events

Once again, intra-winter differences are evident prior to WPVs in Fig.8 (left column). In early winter, the anomalous circulation pattern shows a WN1-like structure with two main centres of action, positive over Greenland and Western Siberia and negative over the Eastern Siberia (Fig.8a). The two anomalous centres are located close to the main climatological ones, Eurasian ridge and Pacific trough, intensifying the climatological structures. The positive values of the interaction term of the eddy heat flux near these areas in Fig.5c confirm the constructive interference between the anomalous and climatological waves. Additionally, the Eurasian ridge and Pacific trough form part of the climatological WN1 wave (Garfinkel et al. 2010) and consequently, the constructive interference of the anomalous and climatological waves likely leads to an enhancement of WN1 wave as already shown in Fig.7a. The anomalous pattern is similar to that shown in Fig.9b of García-Serrano et al. (2015) but for 200 hPa associated with the loss of sea ice concentration at the Barents-Kara Seas region (northeast of Scandinavia) in agreement with the results of the heat flux.

In mid-winter, the anomalous Z_{500} is mainly characterized by a combination of WN1 and WN2 patterns (Fig.8c). As in early winter, the two strongest centres of anomalies are located over Western and Eastern Siberia-Pacific, but the mid-winter pattern also has two weak ones over Canada and Greenland (the latter not statistically significant). The positive anomalies of Z_{500} over Canada are merely in quadrature with the climatological eddies and thus, do not interfere much with them. However, they might be responsible for the anomalous wave activity injection into the stratosphere associated with the anomalous waves only (Fig.5e) as happened during the MSW of January 2009 (Ayarzagüena et al. 2011). The rest of the Z_{500} anomalies interfere constructively with the climatological WN1 and WN2 waves (Garfinkel et al. 2010) and might lead to an enhancement of the WN1 and WN2 wave activity in agreement with Fig.7c. Comparing with the results of Barriopedro and Calvo (2014), the centres of positive anomalies of Z_{500} in mid-winter can be related to blockings over Siberia sector influenced by La Niña events. Blockings over this region enhance WN2 wave activity (Nishii et al. 2011), consistently with the results in Fig.5f.

In late winter, the anomalous structure also shows a combination of WN1 and WN2-like patterns as in mid-winter. However, in this case the centre of negative anomalies over Greenland becomes the strongest one and extends further eastward. As a result, the anomalous low is located close to the climatological trough over Northeastern America and intensifies it. The rest of the positive and negative centres of anomalies of Z_{500}

have weakened and reduced respect to mid-winter, in particular over the Eastern Siberia-Pacific that is now restricted to the Pacific. Nevertheless, they still coincide with the antinodes of the climatological waves and their constructive interference is statistically significant according to Fig.5i.

Subsequently, we have verified the effects of the anomalous circulation on the upward propagating WN1 and WN2 wave activity that we have just inferred in Fig.8. Figure 9 shows the cross-sections of anomalous and climatological eddy geopotential height averaged over 55ºN-75ºN for WN1 (left column) and WN2 (right column) for WPVs. The averaging latitude band corresponds to the region where the main centres of anomalies of Z_{500} and climatological eddy geopotential height are located. Results do not differ much when selecting a different band such as 45ºN-75ºN (not shown). In early winter, as anticipated before, the anomalous WN1 wave is in phase with the climatological wave and propagates upward as denoted by the westward tilt with the height (Fig.9a). Thus, the enhancement of the upward-propagating WN1 wave is verified. At 500 hPa the negative and positive antinodes of the wave coincide with the locations of the anomalous Eastern Siberian low and Greenland and Western Siberian highs identified in Fig.8a. In contrast, the anomalous WN2 wave does not interfere with the climatological wave (Fig.9b). In mid- (Fig.9c and d) and late winter (Fig.9e and f), the anomalous WN1 and WN2 waves are in general in phase with climatological waves and both show westward tilt with height, confirming the intensification of the upward-propagating WN1 and WN2 waves prior to the occurrence of WPVs.

b) SPV events

Contrarily to WPV events, before SPV events (Fig.8, right) in the three winter sub-periods there is a negative centre of Z_{500} anomalies over Western Siberia and a positive centre over Eastern Siberia-Pacific as also shown by Kolstad and Charlton-Perez (2011) for SPVs in the extended winter (DJFM). Both centres are close to the climatological Eurasian ridge and Pacific trough and they tend to diminish the climatological wave pattern. Nevertheless, the centres of anomalies are much weaker in early winter than in the rest of the season. The anomalous high over Eastern Siberia is the main structure leading to the inhibition of wave activity by interaction with the climatological wave in early winter. The result is confirmed by the statistically significant negative values in the interaction term of the heat flux (Fig.6c). A pseudo-negative phase of Pacific-North American pattern is shown in Fig.8d in mid-winter, which is known to weaken the climatological Eastern Siberia-Pacific low and once again, inhibits WN1 component (in agreement with Fig.7 results). Previous

studies have already shown the occurrence of a similar pattern over the Western Pacific prior to a polar stratospheric cooling (Nishii et al. 2010, 2011, Kolstad and Charlton-Perez 2011). In late winter, the negative anomalies of Z_{500} over Central Siberia are more intense than in the other sub-periods (Fig.8f) and the anomalous circulation pattern has a WN1-like shape in opposite phase with the climatological wave (Garfinkel et al. 2010). This would also explain the suppression of WN1 wave activity shown in Fig.7f.

As for WPVs, we have analysed the upward-propagating anomalous and climatological WN1 and WN2 waves of Z (Fig.10) to confirm the conclusions derived from the analysis of anomalous Z_{500}. In the three sub-periods the anomalous WN1 (Fig.10 left column) is in opposite phase with the climatological waves in the troposphere and stratosphere, indicative of the destructive interference of both waves. As for WN2 wave, the anomalous WN2 is in quadrature with the climatological waves in early and late winter. In mid-winter, the anomalous WN2 wave seems to be in phase with the climatological one. In fact, this result is not very surprising since part of the seven days preceding SPVs show an enhancement of WN2 heat flux (Fig.7d). Nevertheless, the suppression of WN1 wave activity is strong enough to counterbalance the effects of WN2.

3.4 Temporal Evolution of Stratospheric Circulation Anomalies

Fig.11 shows the time-height composites of the standardized anomalies of zonal mean zonal wind at 60ºN during 90 days before and after the onset of the extreme events. Fig.11a and Fig.11b represent the composites for WPV and SPV events, respectively, during all the extended winter similarly to Baldwin and Thompson (2009, their Fig.11). WPVs composites for the extended winter are preceded by positive anomalies of zonal wind and after the event onset the zonal wind is reduced (Fig.11a), in agreement with Baldwin and Thompson (2009). The same pattern appears in Fig.11b for SPVs, with the sign of the anomalies inverted and weaker negative anomalies preceding the event. Although Fig.11a and Fig.11b do not present statistically significant anomalies propagating down to the surface after the events, the anomalies remain in the upper troposphere being able to affect the baroclinic activity (Baldwin et al. 2003). The temporal evolution of anomalous zonal wind for WPVs also presents an intra-seasonal variability (Fig.11, left column). WPVs in early winter (Fig.11c) are preceded by weak and non-statistically significant negative anomalies, while mid-winter and late winter WPVs (Fig.11e and Fig.11g) present a larger previous strengthening of the polar vortex. Albers and Birner (2014) showed a similar vortex preconditioning prior to vortex split MSWs, which is in agreement with the important contribution of WN2 wave activity preceding WPVs in the present study. In particular,

Albers and Birner (2014) found that split MSWs are preceded by an anomalously strong vortex without vertical tilt that is wider in the upper stratosphere and narrower in the lower stratosphere. According to their study, the enhancement of gravity and planetary wave drag constrains this former strong vortex about the pole and weakens it. In early winter and mid-winter WPVs significant anomalies reach the troposphere, and this happens earlier for mid-winter anomalies. In late winter negative anomalies remain in the upper troposphere, probably due to the high variability of the springtime troposphere.

Fig.11 (right) shows the evolution of zonal wind anomalies corresponding to SPV events. In contrast to WPV events, prior to SPV events there are no clear opposite-sign anomalies in early and mid-winter (Fig.11d and Fig.11f). This difference is probably due to the fact that the SPV events have a longer time-scale as they are driven by radiative relaxation while wave forcing drives WPV events. However, late winter SPVs are preceded by negative anomalies (Fig.11h), which is consistent with the occurrence of 2 out 4 SPVs after WPVs and the associated reduction of planetary wave propagation (Fig.7f).

4 Summary and conclusions

In this study we have examined the intra-seasonal variability of the anomalous wave activity injection into the stratosphere preceding polar vortex extremes in the NH using ERA-Interim reanalysis data (1979-2011). Particularly, weak (WPV) and strong (SPV) polar vortex events have been grouped in winter sub-periods depending on the date of the onset: early winter (OND), mid-winter (JF) or late winter (MA).

We have identified the patterns prior to the occurrence of polar vortex extremes in each winter sub-period. In general, WPV (SPV) events are associated with constructive (destructive) interference of anomalous wave activity with the climatological patterns in each winter sub-period. The results show clear intra-seasonal differences in the anomalous wave activity preceding both types of extreme events. Overall, mid-winter extreme events are preceded by the strongest wave activity anomalies, whereas the weakest anomalies are observed prior to early winter extreme events. We summarize here the specific features observed for each winter sub-period.

In early winter, the upward wave propagation preceding WPVs (SPVs) is under the influence of a WQBO-like (EQBO-like) structure. The anomalous geopotential pattern at 500 hPa before WPVs (SPVs) represents a WN1-like structure in phase (out of phase) with the climatological wave that increases (inhibits) the upward

WN1 wave propagation. The spatial patterns of the anomalous wave injection into the stratosphere could be related to the stratospheric pathway of the autumn Arctic sea ice influence on the winter Euro-Atlantic climate as recently shown by García-Serrano et al. (2015), although our results are not conclusive in this respect.

Both mid- and late winter WPV events are preceded by a strong vortex with a specific geometry that favours poleward planetary wave propagation, as discussed by Albers and Birner (2014). However, only mid-winter WPVs are influenced by an EQBO-like structure and it is at a lesser extent than in early winter. The anomalous pattern of the vertical wave injection into the stratosphere before WPVs in mid- and late winter has a contribution of WN1 and WN2 wave activity. This is due to the constructive interference between climatological and anomalous waves over the Eastern Siberia-Pacific region and Western Siberia that produces an increase of the upward WN1 and WN2 wave propagation. For mid-winter WPV events the increase in WN2 wave activity might be related to the predominance of La Niña over El Niño conditions, linked to enhanced blockings over Siberia and WN2 wave activity polar stratosphere perturbations (Barriopedro and Calvo 2014). There is a non-linear eddy-eddy interaction that is responsible for the extension of wave activity over Northern Canada in mid-winter.

Regarding SPVs, mid- and late winter events are preceded by a WQBO-like structure, although it is not very evident in Fig.4d and Fig.4f. We also observe that late winter SPV events are preceded by WPV, in agreement with the late winter cooling proposed by Labitzke (1981). The modulation of climatological patterns by anomalous eddies is the main responsible for the reduction in wave activity preceding mid- and late winter SPVs. In both sub-periods, the suppression of wave activity is mainly due to the inhibition of the WN1 component. For instance, the mid-winter SPV events show a negative phase of the Pacific-North American pattern that has been traditionally related to the mentioned reduction of WN1 wave activity (Nishii et al. 2010, 2011, Kolstad and Charlton-Perez 2011).

It is important to note that the relatively short time period covered by the data and the subsequent small number of extreme polar events might be a weakness for the robustness of our results. In order to overcome this shortcoming, we have applied a non-parametric statistical significance test (namely, a Monte Carlo-like test) to provide confidence to our conclusions. Nevertheless, the number of SPV events is particularly small in late winter (only four) and thus we have avoided deriving any important conclusion for this group of events. The use of a much longer dataset might have reduced this problem, but we prefer not to mix pre- and post-

satellite data (more details in Section 2).

Our results support the conclusions of previous studies concerning the different forcings of extreme polar vortex regime and their most effective timing. To the best of our knowledge, the present work constitutes the first analysis of the intra-seasonal variability of the triggering mechanisms of these events. An important implication of this study is that the dynamical behaviour associated with events occurring in mid-winter months cannot be generalized to other winter sub-periods, in particular regarding precursors and wave activity preceding extreme polar vortex events. Our results suggest that considering the intra-seasonal variability of polar vortex extremes can help improve the representation of stratosphere-troposphere interactions in climate models and seasonal forecast systems.

Acknowledgments

The authors are grateful to two anonymous reviewers, whose comments help improve this manuscript. This work was supported by the Spanish Ministry of Economy and Competitiveness (grant number CGL2012-34997). BA is supported by the Natural Environment Research Council (grant number NE/M006123/1). MA acknowledges funding from the NASA ACMAP program. The ERA-Interim reanalysis data were obtained online at http://data-portal.ecmwf.int/data/d/interim_full_moda/. ENSO and QBO indices have been taken from http://www.cpc.ncep.noaa.gov/products/analysis_monitoring/ensostuff/ensoyears_ERSSTv3b.shtml and http://www.cpc.noaa.gov/data/indices/, respectively.

References

Albers JR, Birner T (2014) Vortex preconditioning due to planetary and gravity waves prior to sudden stratospheric warmings. J Atmos Sci 71:4028-4054. doi: 10.1175/JAS-D-14-0026.1

Andrews DG, Holton JR, Leovy CB (1987) Middle Atmosphere Dynamics. Academic Press, pp 489

Ayarzagüena B, Langematz U, Serrano E (2011) Tropospheric forcing of the stratosphere: A comparative study of the two different major stratospheric warmings in 2009 and 2010. J Geophys Res: Atmos 116. doi: 10.1029/2010JD015023

Ayarzagüena B, Langematz U, Meul S, Oberländer S, Abalichin J, Kubin A (2013) The role of climate change and ozone recovery for the future timing of major stratospheric warmings. Geophys Res Lett 40: 2460-2465. doi:10.1002/grl.50477

445 Ayarzagüena B, Orsolini YJ, Langematz U, Abalichin J, Kubin A (2015) The relevance of the location of
446 blocking highs for stratospheric variability in a changing climate. J Climate 28:531-549. doi:
447 10.1175/JCLI-D-14-00210.1
448 Baldwin MP, Edmon Jr HJ, Holton JR (1985) A diagnostic study of eddy-mean flow interactions during
449 FGGE SOP-1. J Atmos Sci 42:1838-1845
450 Baldwin MP, Dunkerton TJ (1999) Propagation of the Arctic Oscillation from the stratosphere to the
451 troposphere. J Geophys Res 104:30937-30946. doi: 10.1029/1999JD900445
452 Baldwin MP, Dunkerton TJ (2001) Stratospheric harbingers of anomalous weather regimes. Science 294:581-
453 584. doi: 10.1126/science.1063315
454 Baldwin MP, Stephenson DB, Thompson DW, Dunkerton TJ, Charlton AJ, O'Neill A (2003) Stratospheric
455 memory and skill of extended-range weather forecasts. Sci 301:636-640. doi: 10.1126/science.1087143
456 Baldwin MP, Thompson DW (2009) A critical comparison of stratosphere–troposphere coupling indices. Q J
457 R Meteorol Soc 135:1661-1672. doi: 10.1002/qj.479
458 Barriopedro D, Calvo N (2014) On the relationship between ENSO, stratospheric sudden warmings, and
459 blocking. J Climate 27:4704-4720. doi: 10.1175/JCLI-D-13-00770.1
460 Butler AH, Polvani LM (2011) El Niño, La Niña, and stratospheric sudden warmings: A reevaluation in light
461 of the observational record. Geophys Res Lett 38. doi: 10.1029/2011GL048084
462 Christiansen B (2001) Downward propagation of zonal mean zonal wind anomalies from the stratosphere to
463 the troposphere: Model and reanalysis. J Geophys Res 106: 27307–27322. doi:
464 10.1029/2000JD000214
465 Christiansen B (2005) Downward propagation and statistical forecast of the near-surface weather. J Geophys
466 Res: Atmos 110 doi: 10.1029/2004JD005431
467 Dee DP, Uppala SM, Simmons AJ, Berrisford P, Poli P, Kobayashi S et al. (2011) The ERA-Interim
468 reanalysis: Configuration and performance of the data assimilation system. Quart J Roy Meteor Soc
469 137:553-597. doi: 10.1002/qj.828
470 Dunkerton TJ (1990) Annual variation of deseasonalized mean flow acceleration in the equatorial lower
471 stratosphere. J Meteor Soc Japan 68: 499-508

Eliassen A, Palm E (1961) On the transfer of energy in stationary mountain waves. Geofysiske Publikasjoner 22:1-23

García-Serrano J, Frankignoul C, Gastineau G, de la Cámara A (2015) On the predictability of the winter Euro-Atlantic climate: lagged influence of autumn Arctic sea-ice. J Climate 28:5195-5216. doi: 10.1175/JCLI-D-14-00472.1

Garfinkel CI, Hartmann DL, Sassi F (2010) Tropospheric precursors of anomalous Northern Hemisphere stratospheric polar vortices. J Climate 23:3282-3299. doi: 10.1175/2010JCLI3010.1

Gray LJ (2003) The influence of the equatorial upper stratosphere on stratospheric sudden warmings. Geophys Res Lett, 30. doi: 10.1029/2002GL016430

Gray LJ, Crooks S, Pascoe C, Sparrow S, Palmer M (2004) Solar and QBO influences on the timing of stratospheric sudden warmings. J Atmos Sci 61:2777-2796

Gomez-Escolar M, Fueglistaler S, Calvo N, Barriopedro D (2012) Changes in polar stratospheric temperature climatology in relation to stratospheric sudden warming occurrence. Geophys Res Lett 39. doi:10.1029/2012GL053632

Holton JR, Tan HC (1980) The influence of the equatorial quasi-biennial oscillation on the global circulation at 50 mb. J Atmos Sci 37:2200-2208

Hu Y, Tung KK (2003) Possible ozone induced long term changes in planetary wave activity in late winter. J Climate 16:3027–3038

Kodera K, Matthes K, Shibata K, Langematz U, Kuroda Y (2003) Solar impact on the lower mesospheric subtropical jet: A comparative study with general circulation model simulations. Geophys Res Lett 30. doi: 10.1029/2002GL016124

Kolstad EW, Charlton-Perez AJ (2011) Observed and simulated precursors of stratospheric polar vortex anomalies in the Northern Hemisphere. Clim Dyn 37:1443-1456. doi:10.1007/s00382-010-0919-7

Labitzke K (1981) Stratospheric-mesospheric midwinter disturbances: A summary of observed characteristics. J Geophys Res 86:9665–9678. doi: 10.1029/JC086iC10p09665

Li Q, Graf HF, Giorgetta MA (2007) Stationary planetary wave propagation in Northern Hemisphere winter-climatological analysis of the refractive index. Atmos Chem and Phys 7:183-200

499 Li Y, Lau NC (2013) Influences of ENSO on stratospheric variability, and the descent of stratospheric
500 perturbations into the lower troposphere. J Climate 26:4725-4748. doi: 10.1175/JCLI-D-12-00581.1
501 Limpasuvan V, Thompson DW, Hartmann DL (2004) The Life Cycle of the Northern Hemisphere Sudden
502 Stratospheric Warming. J Climate 17:2584-2596
503 Manzini E, Giorgetta MA, Esch M, Kornblueh L, Roeckner E (2006) The influence of sea surface
504 temperatures on the Northern winter stratosphere: Ensemble simulations with the MAECHAM5
505 model. J Climate 19:3863-3881
506 Martius O, Polvani LM, Davies HC (2009) Blocking precursors to stratospheric sudden warming events.
507 Geophys Res Lett 36. doi: 10.1029/2009GL038776
508 Newman PA, Rosenfield JE (1997) Stratospheric thermal damping times. Geophys Res Lett 24:433–436. doi:
509 10.1029/96GL03720
510 Nishii K, Nakamura H, Miyasaka T (2009) Modulations in the planetary wave field induced by upward
511 propagating Rossby wave packets prior to stratospheric sudden warming events: A case-study. Quart J
512 Roy Meteor Soc 135:39-52. doi: 10.1002/qj.359
513 Nishii K, Nakamura H, Orsolini YJ (2010) Cooling of the wintertime Arctic stratosphere induced by the
514 western Pacific teleconnection pattern. Geophys Res Lett 37. doi: 10.1029/2010GL043551
515 Nishii K, Nakamura H, Orsolini YJ (2011) Geographical dependence observed in blocking high influence on
516 the stratospheric variability through enhancement and suppression of upward planetary-wave
517 propagation. J Climate 24:6408-6423. doi: 10.1175/JCLI-D-10-05021.1
518 Palmer TN (1981) Diagnostic study of a wavenumber-2 stratospheric sudden warming in a transformed
519 Eulerian-mean formalism. J Atmos Sci 38:844-855
520 Polvani LM, Waugh DW (2004) Upward wave activity flux as a precursor to extreme stratospheric events and
521 subsequent anomalous surface weather regimes. J Climate 17:3548-3554
522 Plumb RA (1985) On the three-dimensional propagation of stationary waves. J Atmos Sci 42:217-229.
523 Quiroz RS (1979) Tropospheric- stratospheric interaction in the major warming event of January- February
524 1979. Geophys Res Lett 6:645-648. doi: 10.1029/GL006i008p00645

525 Scaife AA, Arribas A, Blockley E, Brookshaw A, Clark RT, Dunstone N et al. (2014) Skillful long- range
526 prediction of European and North American winters. Geophys Res Lett 41:2514-2519. doi:
527 10.1002/2014GL059637
528 Smith KL, Kushner PJ (2012) Linear interference and the initiation of extratropical stratosphere-troposphere
529 interactions. J Geophys Res 117. doi: 10.1029/2012JD017587
530 Solomon A (2014) Wave Activity Events and the Variability of the Stratospheric Polar Vortex. J Climate
531 27:7796-7806. doi: 10.1175/JCLI-D-13-00756.1
532 Taguchi M, Hartmann DL (2006) Increased occurrence of stratospheric sudden warmings during El Niño as
533 simulated by WACCM. J Climate 19:324-332
534 White IP, Lu H, Mitchell NJ (2016) Seasonal evolution of the QBO- induced wave forcing and circulation
535 anomalies in the northern winter stratosphere. J Geophys Res: Atmos 121. doi:
536 10.1002/2015JD024507
537 Woollings T, Charlton-Perez A, Ineson S, Marshall AG, Masato G (2010) Associations between stratospheric
538 variability and tropospheric blocking. J Geophys Res 115. doi: 10.1029/2009JD012742

Figure captions

Fig.1 a) Daily percentiles of the zonal mean zonal wind at 10 hPa and 60ºN (in ms^{-1}) for the period 1979-2011 through the extended winter (October-April). Bottom and top red lines indicate the 15th and 85th percentiles, respectively, and the blue line represents the 50th percentile. b) Distribution of WPV events in early, mid- and late winter (OND, JF and MA, respectively) on basis of ENSO conditions and direction of equatorial zonal wind at 50 hPa, i.e., phase of QBO. c) as b) but for SPV events

Fig.2 Climatology of E-P flux and its divergence in (a) extended winter (ONDJFMA), (b) early winter (OND), (c) mid-winter (JF) and (d) late winter (MA) (1979-2011). E-P flux is represented by vectors with a scale of $5\times10^{8} m^{3}s^{-2}$. Shading illustrates the climatological divergence of E-P flux in units of $ms^{-1}day^{-1}$ and contours represent climatological zonal mean zonal wind in ms^{-1}

Fig.3 Climatology of the meridional eddy heat flux at 100 hPa ($ms^{-1}K$) in (a) extended winter (ONDJFMA), (b) early winter (OND), (c) mid-winter (JF) and (d) late winter (MA) (1979-2011)

Fig.4 Latitude-height composites of the anomalous E-P flux (arrows), its anomalous divergence (shading) and anomalous zonal mean zonal wind (contours) the week prior to the WPV (left column) and SPV events (right column) with statistical significance at a 95% confidence level (Monte Carlo-like test, 5000 random samples). a-b) Composites for 15 WPV and 17 SPV events in early winter, respectively; c-d) composites for 9 WPV and 11 SPV events in mid-winter, respectively; and e-f) composites for 9 WPV and 4 SPV events in late winter, respectively. Arrows with a scale of 3×10^{8} $m^{3}s^{-2}$ are drawn when the value of the vertical component (F_z) of anomalous E-P flux is statistically significant. Color shading illustrates the statistically significant anomalous divergence of E-P flux in units of $ms^{-1}day^{-1}$. Zonal mean zonal wind anomalies (ms^{-1}) are shown in black contours and those statistically significant are highlighted in yellow contours

Fig.5 Composites of the anomalous meridional eddy heat flux ($ms^{-1}K$) at 100 hPa (left column) and its contributor terms (middle and right columns) for the week prior to the occurrence of WPV events. Rows show the results corresponding to the three winter sub-periods: 15 events in early winter (upper), 9 events in mid-winter (middle) and 9 events in late winter (bottom). Dotted regions show statistically significant values at a 95% confidence level (Monte Carlo-like test, 5000 random samples)

Fig.6 As Figure 5 but for the SPV events: 17 events in early winter (upper), 11 events in mid-winter (middle)

and 4 events in late winter (bottom)

Fig.7 Composites of the time evolution of anomalous meridional heat flux $(v'T')_a$ at 100 hPa averaged over 45ºN-75ºN from 15 days before to 15 days after the occurrence of WPV (left column) and SPV events (right column). It has been performed for different zonal wavenumbers: k=1 (red line), k=2 (green line) and the sum of all zonal wavenumbers (blue line). Rows show the results corresponding to the three winter sub-periods: early winter (upper), mid-winter (middle) and late winter (bottom). Asterisk denotes statistically significant values at a 95% confidence level (Monte Carlo-like test, 5000 random samples)

Fig.8 Composites of anomalous geopotential height (gpm) at 500 hPa (shading) for the week prior to the occurrence of WPV (left column) and SPV events (right column). Rows show the results corresponding to the three winter sub-periods: early winter (upper), mid-winter (middle) and late winter (bottom). Dotted regions show statistically significant values of geopotential anomalies at a 95% confidence level (Monte Carlo-like test, 5000 random samples). Grey (negative) and orange (positive) contours represent climatological eddy geopotential height at the same level during these winter sub-periods. The contour interval is 30 gpm

Fig.9 Composites of WN1 (left column) and WN2 (right column) components of anomalous geopotential height averaged over 55ºN-75ºN the week prior to the occurrence of WPV (gpm, shading). Rows show the results corresponding to the three winter sub-periods: early winter (upper), mid-winter (middle) and late winter (bottom). Dotted regions show statistically significant values of eddy geopotential anomalies at a 95% confidence level (Monte Carlo-like test, 5000 random samples). Dashed black (negative) and solid black (positive) contours represent climatological WN1 and WN2 components of geopotential height during these winter sub-periods

Fig.10 As Figure 9 but for SPV events

Fig.11 Height-time composites of standardized anomalies of zonal mean zonal wind at 60ºN around the onset of WPV (left column) and SPV (right column) events, from 90 days before to 90 days after, a-b) for all events through the extended winter, c-d) for early winter events, e-f) for mid-winter events and g-h) for late winter events. Statistically significant values at a 95% confidence level are dotted (Monte Carlo-like test, 5000 random samples)

Tables

Table 1 Central date of WPV and SPV events identified in ERA-Interim during the winter period 1979-2011

Central date of WPV (33 events)	Central date of SPV (32 events)
23 Nov 1979	16 Jan 1980
28 Feb 1980	28 Nov 1980
01 Dec 1981	17 Apr 1981
16 Apr 1982	18 Nov 1982
24 Feb 1984	03 Jan 1983
27 Dec 1984	27 Oct 1983
24 Mar 1985	21 Jan 1984
20 Mar 1986	09 Dec 1985
20 Jan 1987	19 Oct 1986
19 Nov 1987	24 Jan 1988
20 Feb 1989	07 Oct 1988
22 Mar 1992	19 Dec 1988
02 Apr 1994	22 Dec 1989
11 Apr 1996	26 Oct 1990
16 Nov 1996	17 Dec 1991
18 Dec 1997	23 Jan 1993
11 Dec 1998	14 Feb 1994
25 Feb 1999	29 Nov 1994
11 Nov 2000	01 Mar 1995
06 Feb 2001	05 Feb 1996
21 Dec 2001	27 Jan 1997
17 Apr 2003	22 Oct 1997
26 Dec 2003	06 Jan 2000
25 Oct 2004	03 Apr 2001
11 Mar 2005	26 Oct 2001
21 Oct 2005	07 Nov 2002
07 Jan 2006	12 Jan 2005
17 Oct 2006	10 Dec 2004
10 Oct 2007	23 Dec 2007
23 Jan 2009	30 Dec 2008
06 Nov 2009	27 Mar 2009
26 Jan 2010	08 Feb 2011
05 Apr 2011	

Figure1

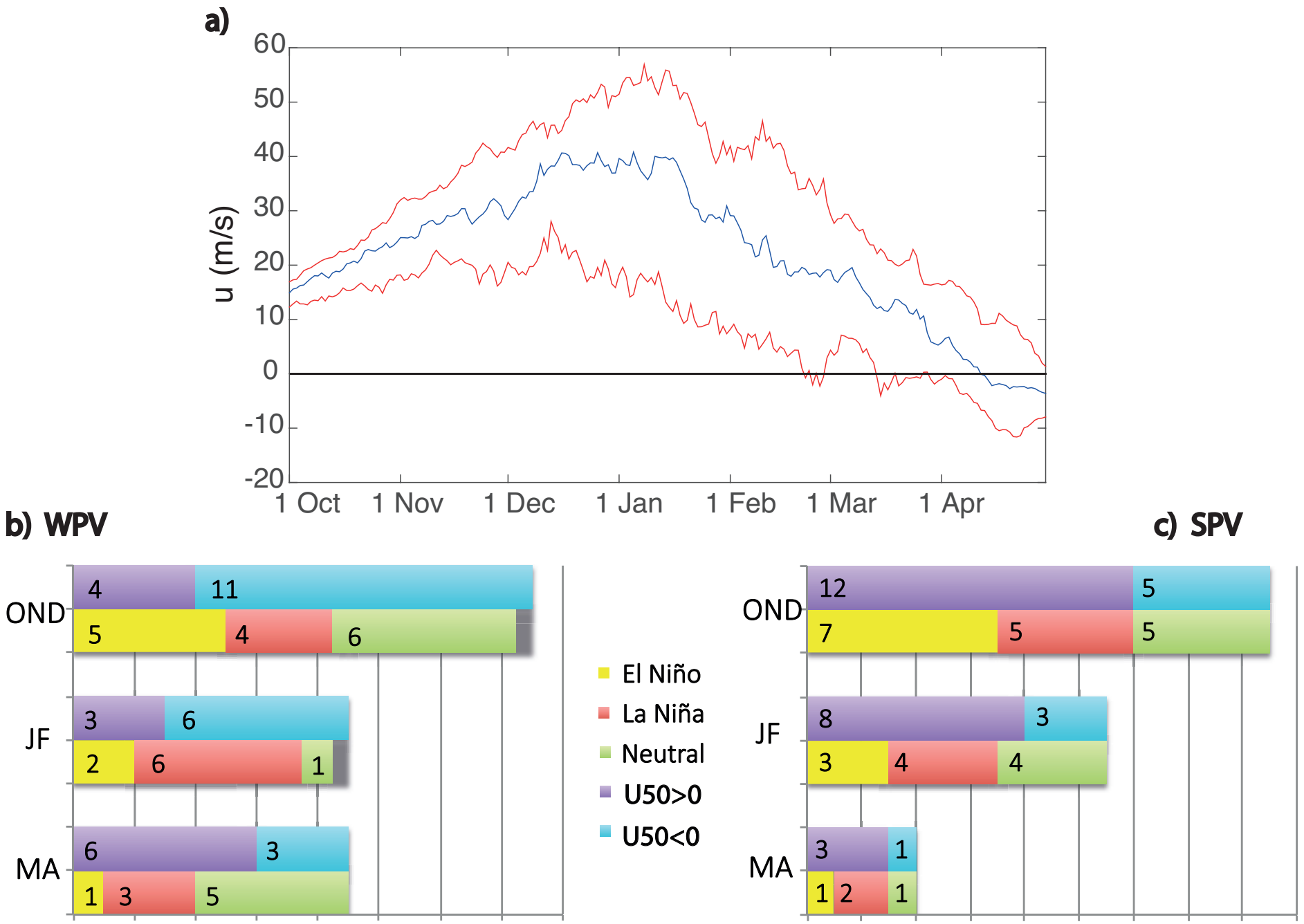
a)
60
50
40
30
20
10
0
-10
-20
u (m/s)
1 Oct
1 Nov
1 Dec
1 Jan
1 Feb
1 Mar
1 Apr
b) WPV
OND
4
11
5
4
6
JF
3
6
2
6
1
MA
6
3
1
3
5
El Niño
La Niña
Neutral
U50>0
U50<0
c) SPV
OND
12
5
7
5
5
JF
8
3
3
4
4
MA
3
1
1
2
1

Figure2

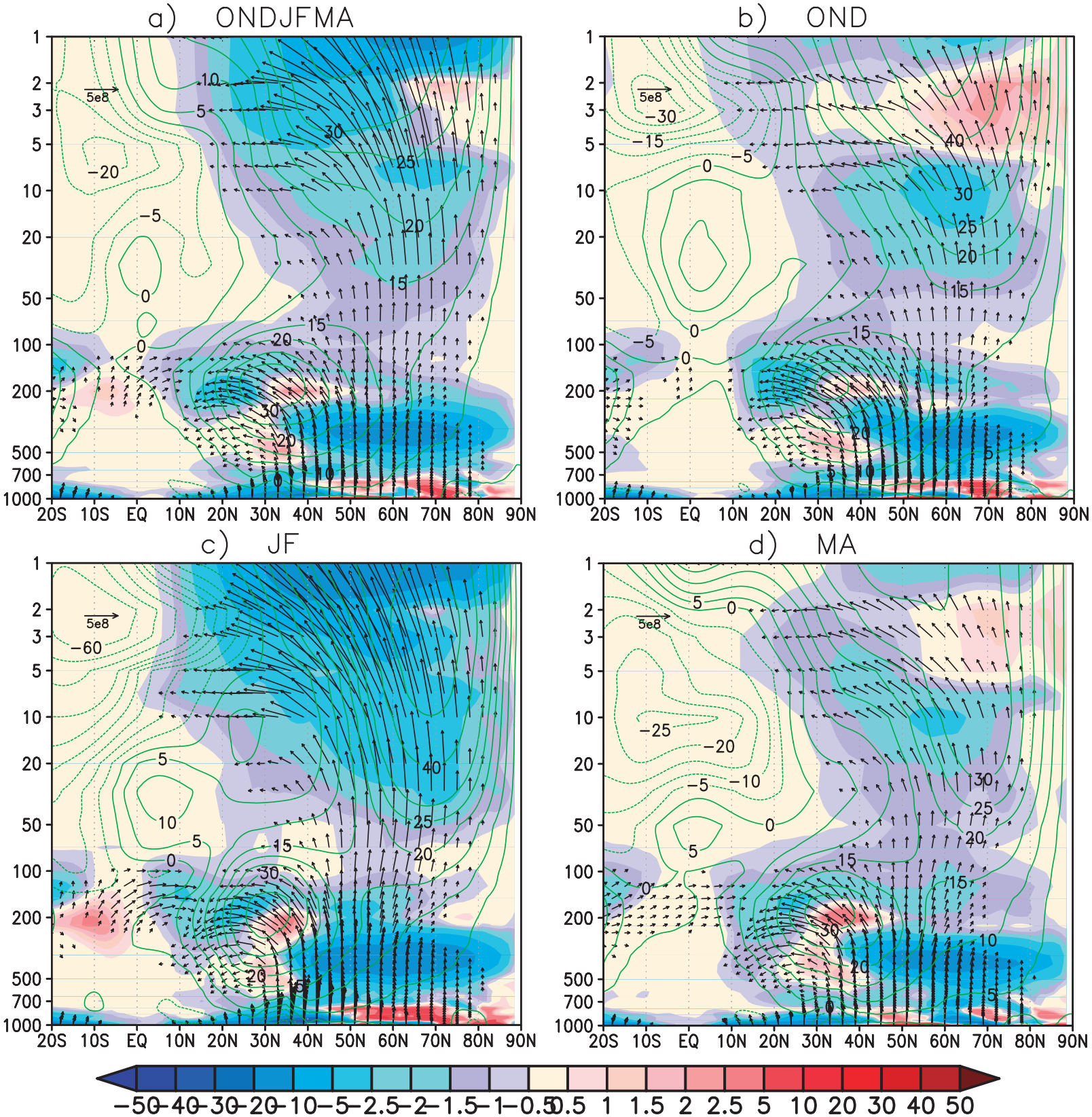
a) ONDJFMA
b) OND
c) JF
d) MA
5e8
1
2
3
5
10
20
50
100
200
500
700
1000
20S 10S EQ 10N 20N 30N 40N 50N 60N 70N 80N 90N
−50 −40 −30 −20 −10 −5 −2.5 −2 −1.5 −1 −0.5 0.5 1 1.5 2 2.5 5 10 20 30 40 50

Figure3

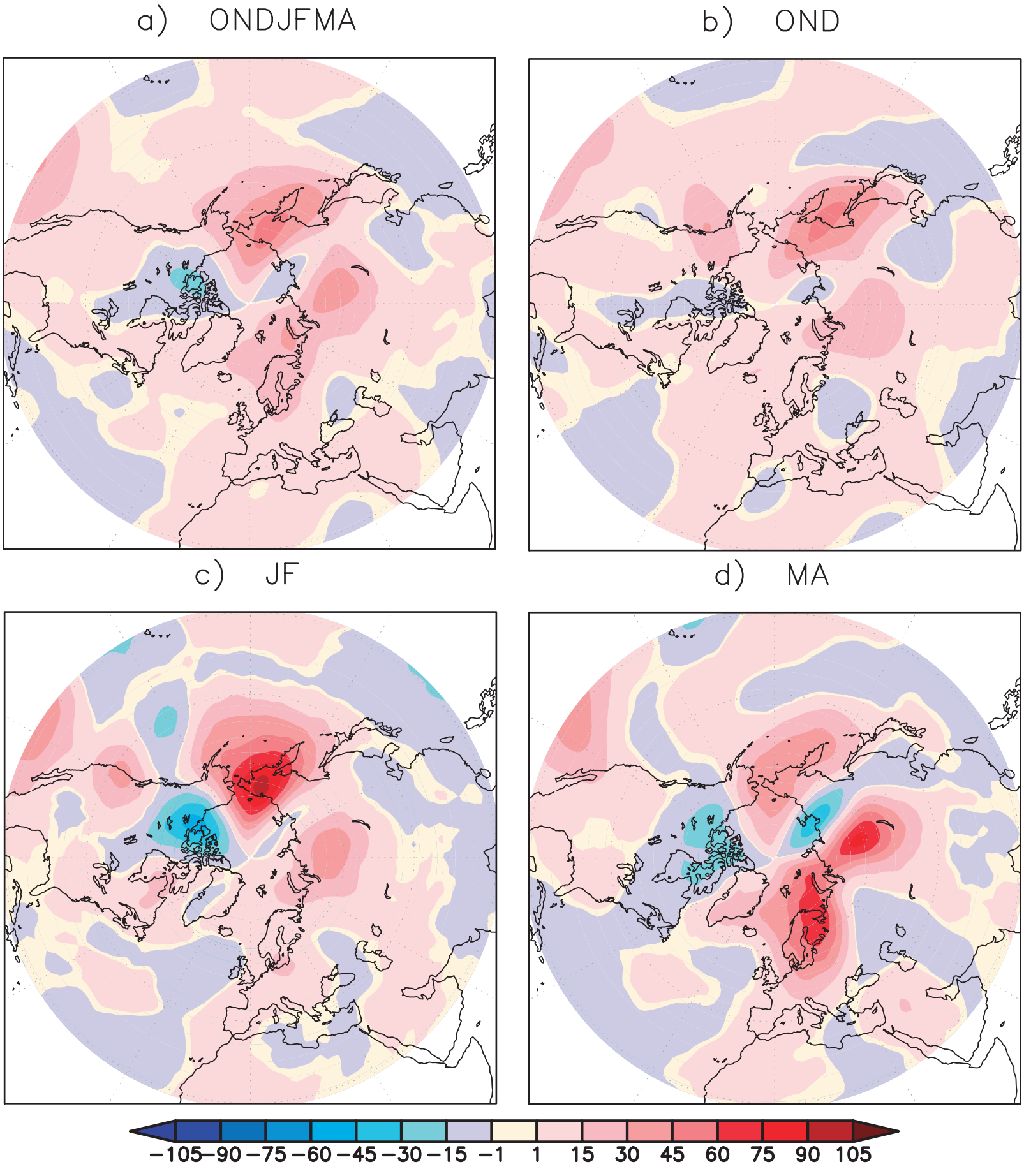
a) ONDJFMA
b) OND
c) JF
d) MA
−105 −90 −75 −60 −45 −30 −15 −1 1 15 30 45 60 75 90 105

Figure4

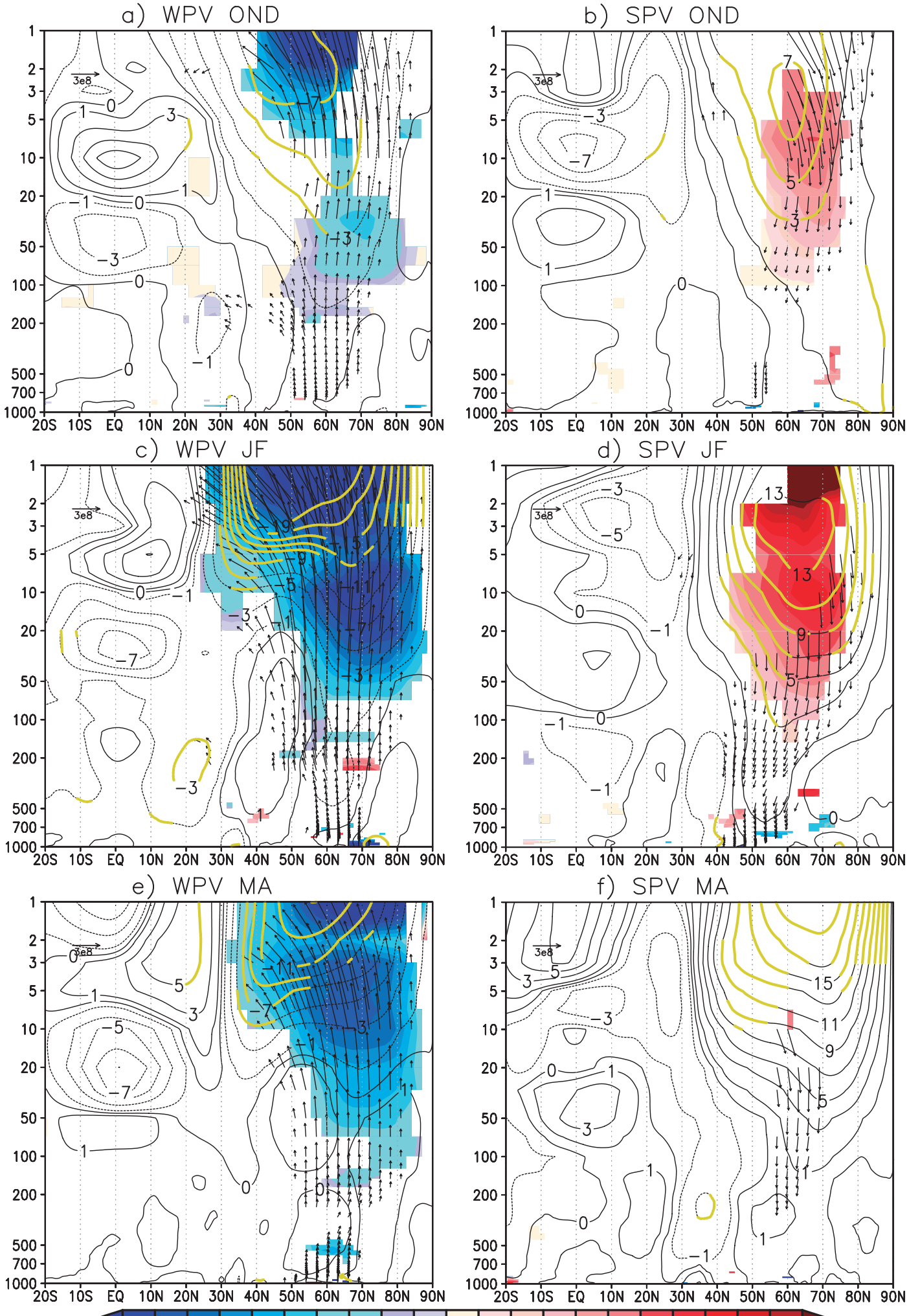
a) WPV OND
b) SPV OND
c) WPV JF
d) SPV JF
e) WPV MA
f) SPV MA
3e8
1 2 3 5 10 20 50 100 200 500 700 1000
20S 10S EQ 10N 20N 30N 40N 50N 60N 70N 80N 90N
−8 −7 −6 −5 −4 −3 −2 −1.5 −1 −0.8 −0.5 0.5 0.8 1 1.5 2 3 4 5 6 7 8

Figure5

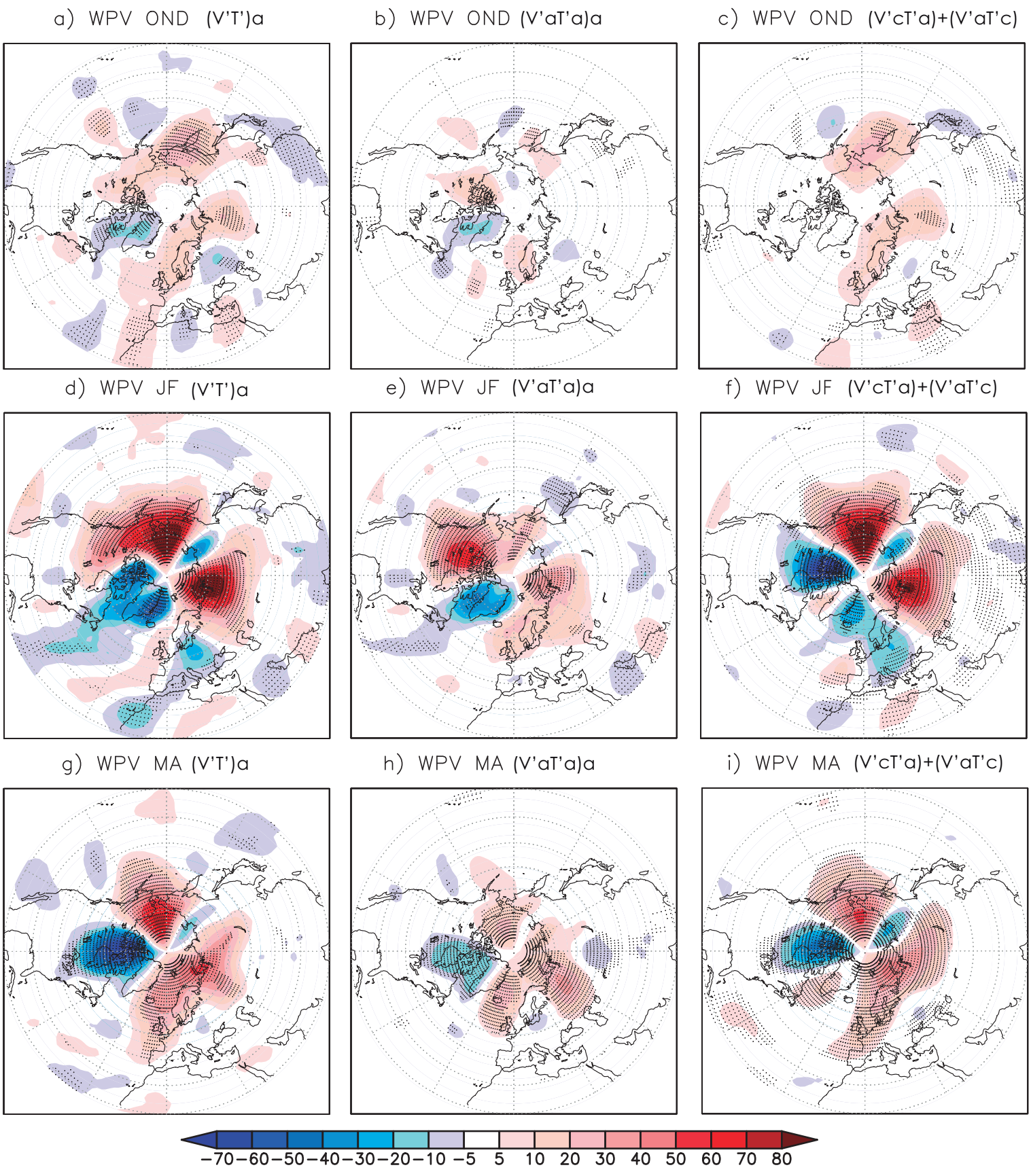
a) WPV OND (V'T')a
b) WPV OND (V'aT'a)a
c) WPV OND (V'cT'a)+(V'aT'c)
d) WPV JF (V'T')a
e) WPV JF (V'aT'a)a
f) WPV JF (V'cT'a)+(V'aT'c)
g) WPV MA (V'T')a
h) WPV MA (V'aT'a)a
i) WPV MA (V'cT'a)+(V'aT'c)
−70 −60 −50 −40 −30 −20 −10 −5 5 10 20 30 40 50 60 70 80

Figure6

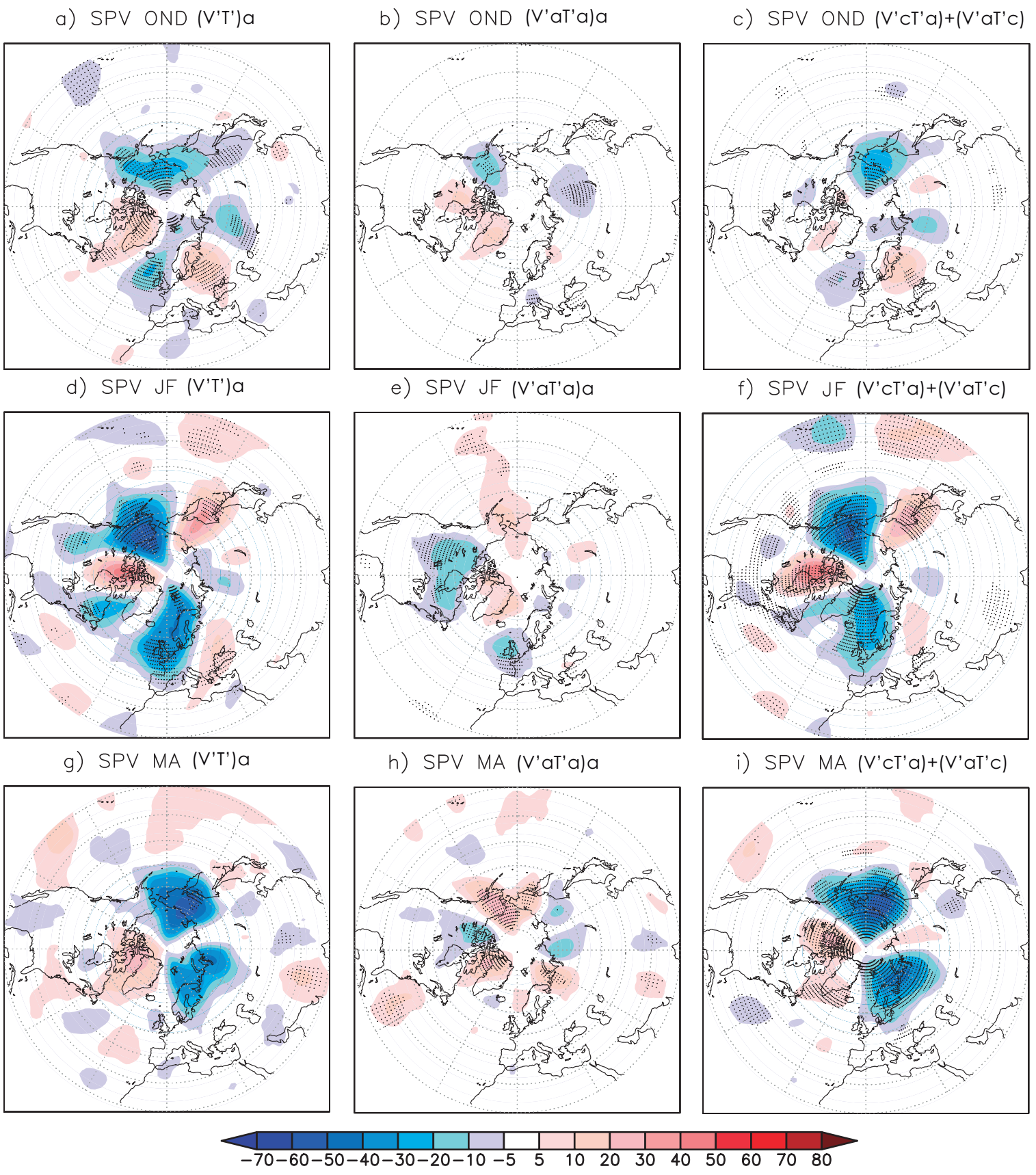
a) SPV OND (V'T')a
b) SPV OND (V'aT'a)a
c) SPV OND (V'cT'a)+(V'aT'c)
d) SPV JF (V'T')a
e) SPV JF (V'aT'a)a
f) SPV JF (V'cT'a)+(V'aT'c)
g) SPV MA (V'T')a
h) SPV MA (V'aT'a)a
i) SPV MA (V'cT'a)+(V'aT'c)
−70 −60 −50 −40 −30 −20 −10 −5 5 10 20 30 40 50 60 70 80

Figure7

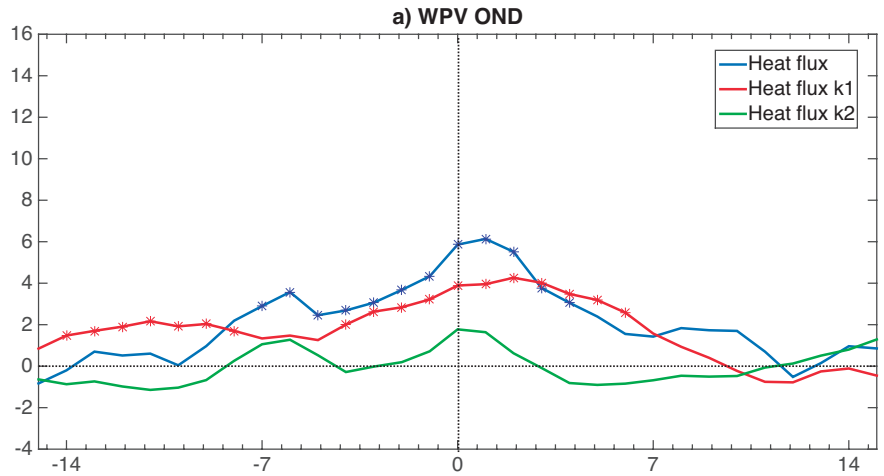
a) WPV OND
Heat flux
Heat flux k1
Heat flux k2

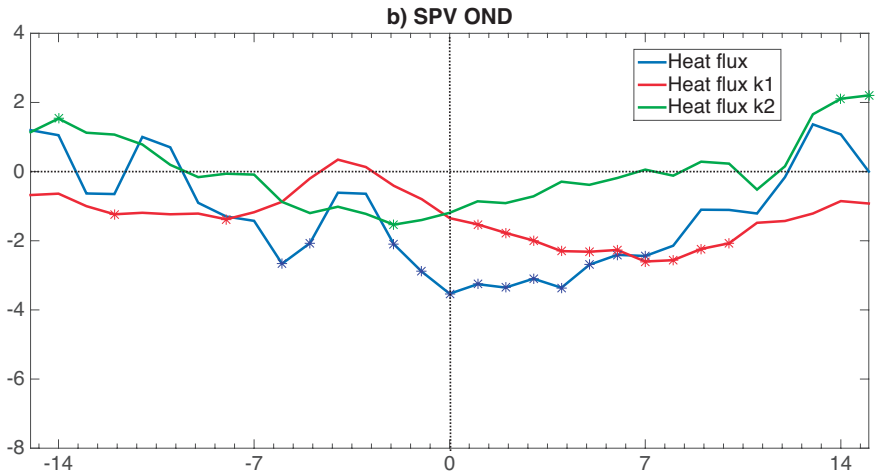
b) SPV OND
Heat flux
Heat flux k1
Heat flux k2

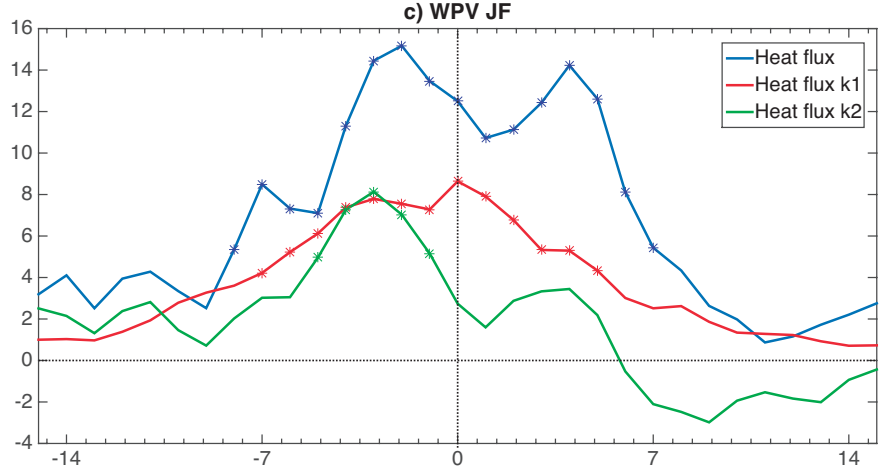
c) WPV JF
Heat flux
Heat flux k1
Heat flux k2

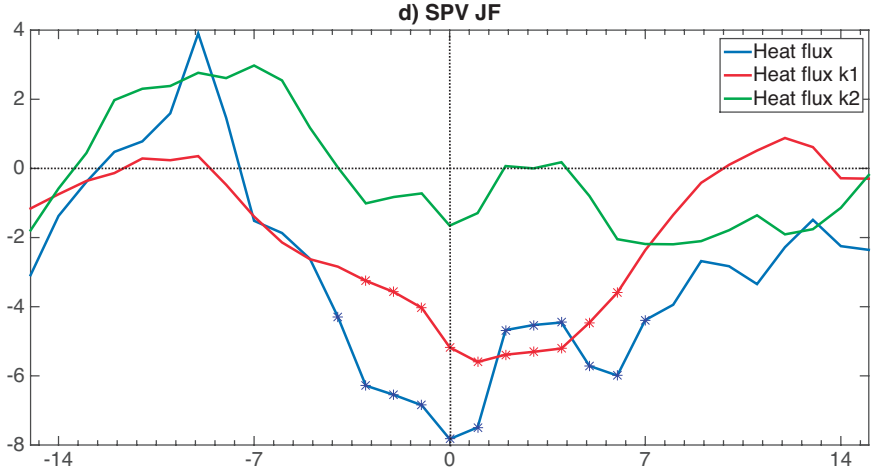
d) SPV JF
Heat flux
Heat flux k1
Heat flux k2

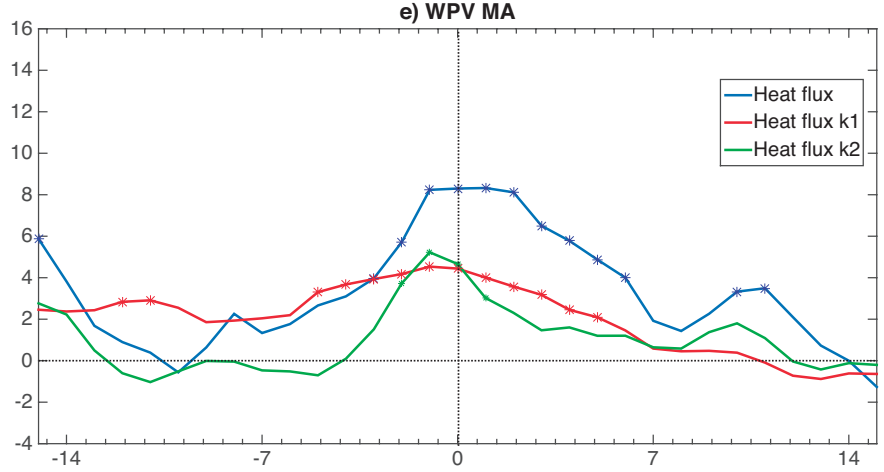
e) WPV MA
Heat flux
Heat flux k1
Heat flux k2

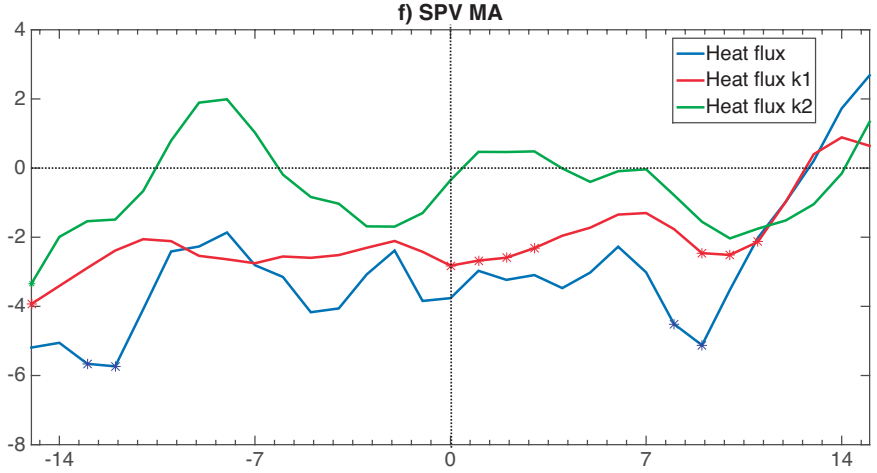
f) SPV MA
Heat flux
Heat flux k1
Heat flux k2

Figure8

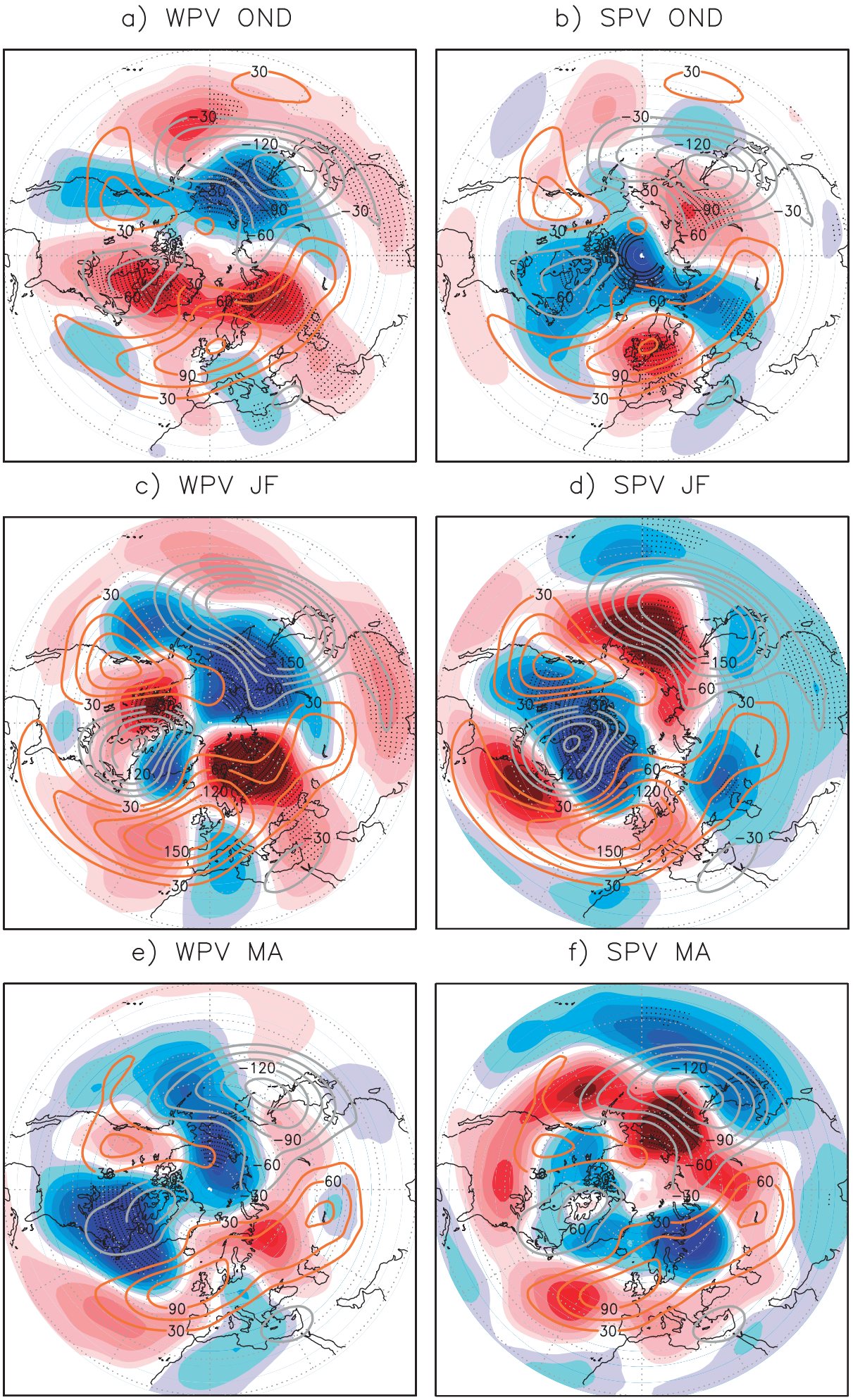
a) WPV OND
b) SPV OND
c) WPV JF
d) SPV JF
e) WPV MA
f) SPV MA
−70 −60 −50 −40 −30 −20 −10 −5 5 10 20 30 40 50 60 70

Figure9

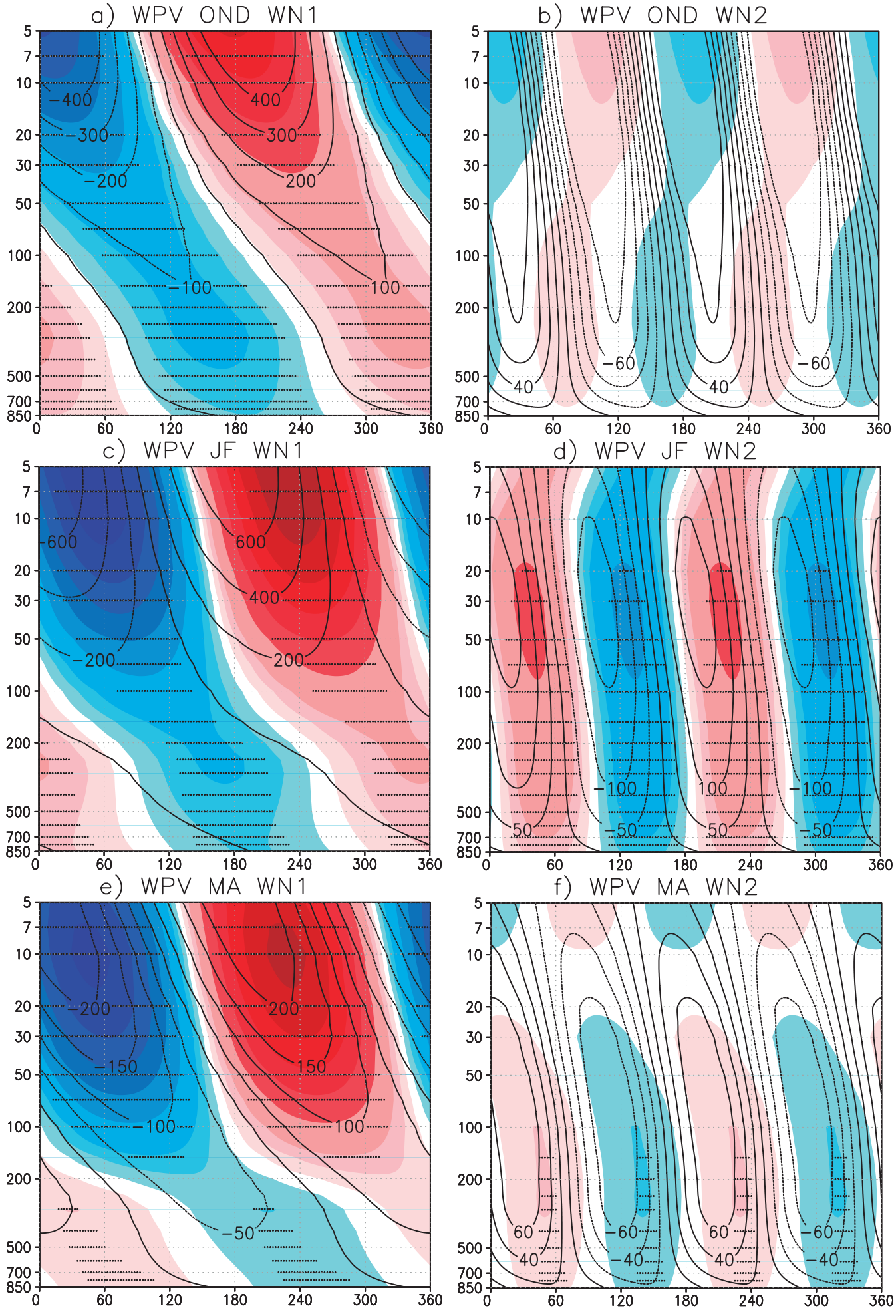
a) WPV OND WN1
b) WPV OND WN2
c) WPV JF WN1
d) WPV JF WN2
e) WPV MA WN1
f) WPV MA WN2
5
7
10
20
30
50
100
200
500
700
850
0
60
120
180
240
300
360
−300 −250 −200 −150 −100 −50 −30 −10 10 30 50 100 150 200 250 300

Figure10

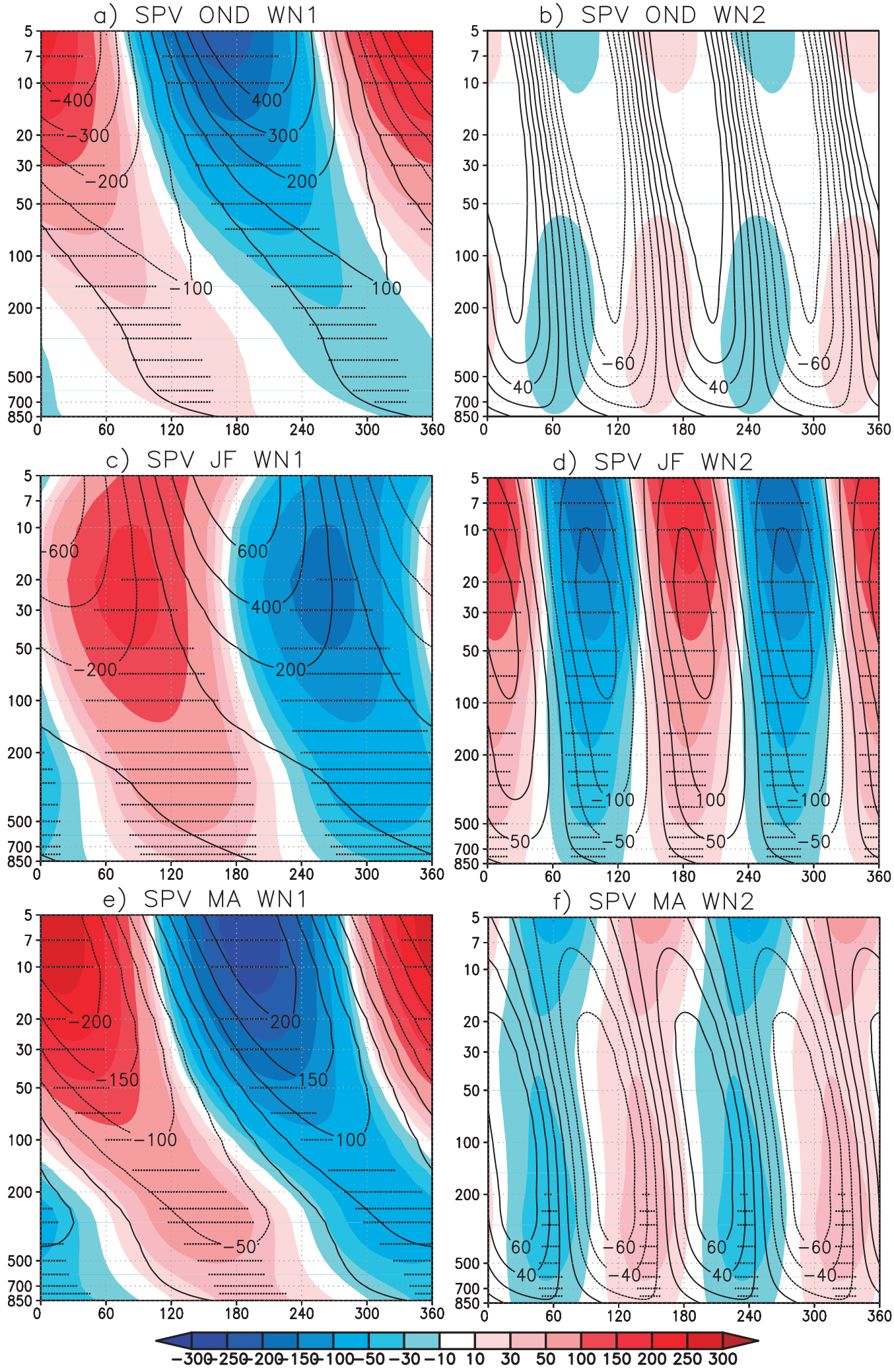
a) SPV OND WN1
b) SPV OND WN2
c) SPV JF WN1
d) SPV JF WN2
e) SPV MA WN1
f) SPV MA WN2
5
7
10
20
30
50
100
200
500
700
850
0
60
120
180
240
300
360
−300 −250 −200 −150 −100 −50 −30 −10 10 30 50 100 150 200 250 300

Figure11

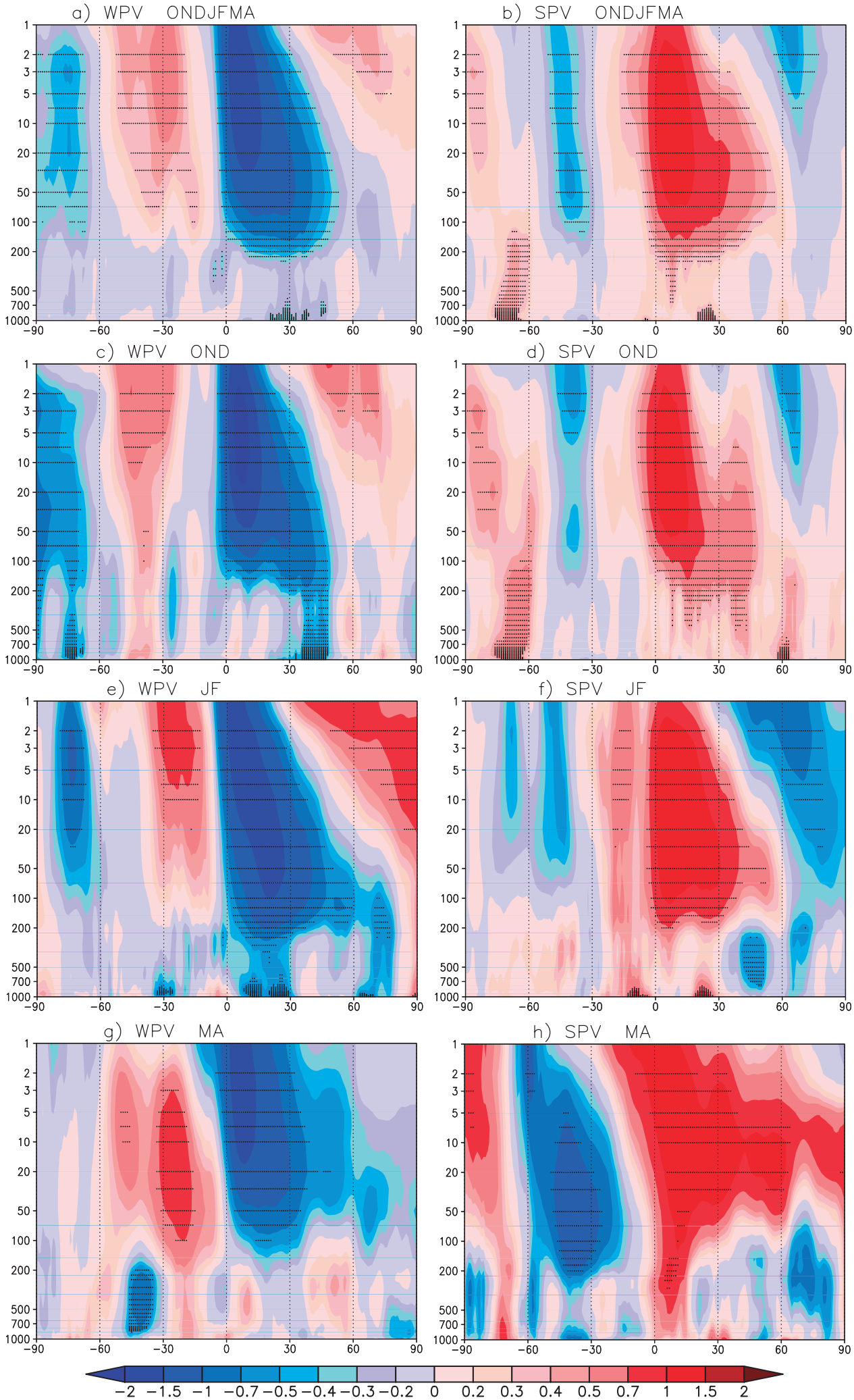
a) WPV ONDJFMA
b) SPV ONDJFMA
c) WPV OND
d) SPV OND
e) WPV JF
f) SPV JF
g) WPV MA
h) SPV MA
1
2
3
5
10
20
50
100
200
500
700
1000
−90
−60
−30
0
30
60
90
−2 −1.5 −1 −0.7 −0.5 −0.4 −0.3 −0.2 0 0.2 0.3 0.4 0.5 0.7 1 1.5 2